

pubs.acs.org/est Article

# **Tellurite Adsorption onto Bacterial Surfaces**

Jennifer L. Goff, Yuwei Wang, Maxim I. Boyanov, Qiang Yu, Kenneth M. Kemner, Jeremy B. Fein, and Nathan Yee\*



Cite This: Environ. Sci. Technol. 2021, 55, 10378-10386



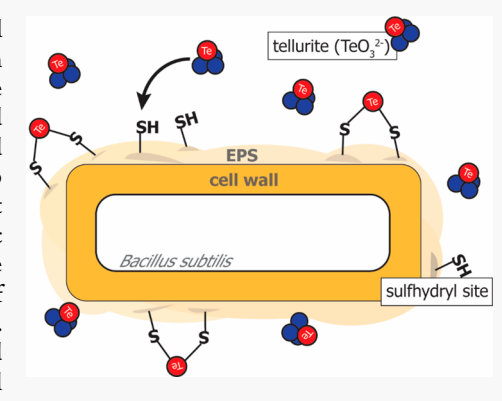
**ACCESS** 

III Metrics & More



SI Supporting Information

ABSTRACT: Tellurium (Te) is an emerging contaminant and its chemical transformation in the environment is strongly influenced by microbial processes. In this study, we investigated the adsorption of tellurite [Te(IV), TeO<sub>3</sub><sup>2-</sup>] onto the common soil bacterium *Bacillus subtilis*. Thiol-blocking experiments were carried out to investigate the role of cell surface sulfhydryl sites in tellurite binding, and extended X-ray absorption fine structure (EXAFS) spectroscopy was performed to determine the chemical speciation of the adsorbed tellurite. The results indicate that tellurite reacts with sulfhydryl functional groups in the extracellular polymeric substances (EPS) produced by *B. subtilis*. Upon binding to sulfhydryl sites in the EPS, the Te changes from Te–O bonds to Te–S coordination. Further analysis of the surface-associated molecules shows that the EPS of *B. subtilis* contain proteins. Removal of the proteinaceous EPS dramatically decreases tellurite adsorption and the sulfhydryl surface site concentration. These findings indicate that sulfhydryl binding in EPS plays a key role in tellurite adsorption on bacterial surfaces.



KEYWORDS: tellurium, metalloid, extracellular polymeric substances, CdTe, photovoltaic, sulfhydryl, toxicity, X-ray adsorption spectroscopy

# **■** INTRODUCTION

Tellurium (Te) is a chalcogen used in photovoltaic technologies for the production of low-cost cadmium telluride (CdTe) solar cells and the disposal of CdTe solar panels contributes to environmental contamination when soluble Te is released from buried waste. Upon decommissioning and disposal of CdTe photovoltaic devices, Te undergoes redox transformations that form dissolved tellurite [Te(IV), TeO $_3^{2-}$ ] and tellurate [Te(VI), TeO $_4^{2-}$ ] in landfill leachate. Tellurite is more toxic than tellurate to the microorganisms involved in biodegradation, and the accumulation of tellurite in landfill leachate causes the inhibition of acetoclastic and hydrogenotrophic methanogenesis. Because tellurite is also toxic to humans, there is significant interest in understanding its environmental fate and transport to drinking water sources.

Microbial interactions can alter the chemical speciation of tellurite in the environment. Diverse microorganisms are able to reduce tellurite to elemental tellurium [Te(0)] and precipitate nanoparticulate Te rods and spheres. Microbes also uptake tellurite into their cells, 13–15 where it interacts with intracellular thiols and depletes cytoplasmic reservoirs of glutathione. Furthermore, experimental studies with other organisms have shown that tellurite binds to proteins and reacts with cellular enzymes that contain sulfhydryl functional groups.

Bacterial cell surfaces are known to harbor sulfhydryl functional groups<sup>20,21</sup> that adsorb environmental contami-

nants, <sup>22–25</sup> including selenium (Se), <sup>26</sup> a chalcogen that is chemically similar to Te. A recent spectroscopic investigation by Yu et al. <sup>26</sup> revealed that selenite [Se(IV), SeO<sub>3</sub> <sup>2–</sup>] binds to bacterial surface thiol sites via the formation of R<sub>1</sub>S–Se–SR<sub>2</sub> organo-selenium complexes. Thiol site densities on bacterial surfaces are generally low, but sulfhydryl-selenium complexes are significantly more stable than Se adsorbed to carboxyl and phosphoryl functional groups. <sup>27</sup> Thus, at environmentally relevant contaminant concentrations, sulfhydryl functional groups on cell surfaces can control bacterial adsorption reactions. <sup>28</sup> Currently, the molecules on bacterial surfaces that host reactive sulfhydryl functional groups are poorly understood, and the adsorption of tellurite onto bacterial cells has not been characterized.

The objective of this study was to examine the mechanism of tellurite binding onto bacterial surfaces. Because tellurite reacts with sulfhydryl-containing molecules, <sup>29,30</sup> and the common soil bacterial species *Bacillus subtilis* is known to produce cell surface sulfhydryl sites, <sup>21,23,26</sup> we selected *B. subtilis* to test the hypothesis that bacterial tellurite adsorption is controlled by

Received: February 10, 2021 Revised: May 16, 2021 Accepted: July 6, 2021 Published: July 19, 2021





cell surface thiols. We conducted thiol-blocking experiments to investigate the role of cell surface sulfhydryl sites in tellurite binding, and we performed X-ray absorption near edge structure (XANES) spectroscopy and extended X-ray absorption fine structure (EXAFS) spectroscopy to determine the chemical speciation of the adsorbed Te. The results indicate that sulfhydryl-containing molecules in extracellular polymeric substances (EPS) play a key role in tellurite adsorption onto bacterial surfaces.

#### MATERIALS AND METHODS

Preparation of Bacterial Cells. Bacillus subtilis strain 168 was grown at 32 °C in an enriched trypticase soy broth (TSB) medium containing 30 g/L of TSB and 5 g/L of yeast extract. Overnight cultures were transferred to 1 L of the growth medium and incubated for up to 24 h while shaken at 60 rpm. The cells were then harvested by centrifugation at  $8100 \times g$ and washed three times with a 0.1 M NaCl electrolyte solution to remove soluble thiols and growth medium components from the cell surface. Although B. subtilis is a prolific sporeformer, initiation of spore formation requires nutrient-starved conditions.<sup>31</sup> As the cultures were never harvested beyond early stationary phase, the extent of spore formation was negligible. The absence of spores was verified by light microscopy before experimentation.

Experiments were conducted to investigate the role of EPS and cell surface thiols in tellurite adsorption. To detach the EPS from B. subtilis surfaces, cell suspensions were mixed with a cation exchange resin<sup>20</sup> (Dowex Marathon C sodium form or Amberlite HPR1100 sodium form, 20-50 mesh) at a resin/0.1 M NaCl/biomass ratio of  $\sim 30/30/1$  by mass. After stirring the suspension for 2 h, the resin was allowed to settle and the supernatant containing the cells and the EPS was collected. The supernatant was then centrifuged  $8100 \times g$  for 10 min to separate the cells and the detached EPS material.

To investigate the role of cell surface thiols in tellurite adsorption, sulfhydryl sites on the cell surface were selectively blocked using the membrane-impermeable thiol-specific fluorescent probe monobromo(trimethylammonio)-bimane bromide(qBBr) (Toronto Research Chemicals).<sup>32</sup> Washed cell pellets were resuspended in 30 mL 0.1 M NaCl solution and incubated with qBBr (100  $\mu$ M) for 2 h. The cell suspensions were centrifuged at 8100 × g for 15 min and subsequently washed three times in 0.1 M NaCl solution with centrifugation steps at  $8100 \times g$  for 15 min.

Tellurite Adsorption Experiments. Adsorption experiments were conducted with washed cells, resin-treated cells, and qBBr-treated cells. For all experiments, cell pellets were resuspended in 0.1 M NaCl (pH  $7.2 \pm 0.1$ ) and diluted to a final wet biomass concentration of 20 g/L. Cell suspensions were then dispensed into individual batch reactors and reacted with known amounts of disodium tellurite (10-80  $\mu$ M). Tellurite concentrations for this study were selected based on their relevance to Te concentrations measured at contaminated sites. Qin et al. (2017) reported that abandoned mine tailings from a gold and silver mine in Japan contained 10.2 to 18.0 ppm total Te<sup>7</sup> and Perkins (2011) reported 0.02 to 11.12 ppm total Te in soils surrounding a nickel refinery in the United Kingdom.<sup>33</sup> Our reactors contained approximately 1 to 10 ppm Te. After the reactors were shaken at 60 rpm for 3 h, the cell suspensions were filtered using 0.22  $\mu$ m nylon filters and the filtrate was acidified with 2% HNO3. The dissolved Te concentration in the filtrate was measured using inductively

coupled plasma optical emission spectroscopy (ICP-OES) using an iCAP 7400 ICP-OES analyzer (Thermo Fisher) at a wavelength of 214.282 nm. Matrix-matched standards were prepared with dilutions of a disodium tellurite solution. The amount of tellurite adsorption was determined by calculating the difference between the initial Te concentration and Te concentration analyzed in the filtrate.

Protein and Thiol Concentrations in EPS. The concentration of proteins in the EPS was measured using the Pierce Modified Lowry Protein Assay.<sup>34</sup> Briefly, 1 mL of modified Lowry Reagent was added to 0.2 mL of the sample and allowed to react at room temperature. After 10 min, 100  $\mu L$  of 1× Folin-Ciocalteu Reagent was added and the sample was incubated at room temperature for another 30 min. The absorbance of the sample was then measured spectrophotometrically at 750 nm. All experiments were conducted in triplicate. Bovine serum albumin (BSA) protein was used to produce standards for the calibration curve.

To investigate the thiol concentrations in EPS, cells from early stationary phase cultures were harvested. The thiol concentration in the EPS was quantified by sulfhydryl (R-SH) specific derivatization followed by fluorescence spectroscopy.<sup>32</sup> The EPS were reacted with the fluorophore monobromobimane (mBBr) (Invitrogen) which forms thioether bonds with reduced thiol moieties to generate fluorescence.<sup>35</sup> Disulfide bonds are not reactive with mBBr and thus the fluorophore is specific to the R-SH moiety. The EPS were diluted in 0.1 M NaCl and reacted with a known amount of freshly prepared mBBr reagent. After 2 h of reaction in the dark, the fluorescence was measured using a microplate reader (Molecular Devices) at Ex/Em 394/490 nm. Duplicate experiments were conducted. A control experiment with a blank 0.1 M NaCl solution was performed to determine the background fluorescence of mBBr.

Potentiometric Titrations. Acid-base titrations and surface complexation modeling were used to determine the total proton-active site concentration on the cell surface. <sup>21</sup> The concentration of thiol sites was determined by measuring the decrease in the concentration of total binding sites after the thiol sites were selectively blocked using qBBr. In order to block thiol sites and eliminate the deprotonation activity of sulfhydryl functional groups, cells were suspended in a freshly prepared qBBr solution in 0.1 M NaCl with pH buffered to 7.0 ± 0.1 using a 1.8 mM Na<sub>2</sub>HPO<sub>4</sub>/18.2 mM NaH<sub>2</sub>PO<sub>4</sub> buffer, with a qBBr/biomass ratio of approximately 100  $\mu$ mol/1 g for 2 h, followed by three biomass washes with a 0.1 M NaCl electrolyte solution. Potentiometric titrations of cells with and without qBBr treatment were conducted using an autotitrator assembly with ~10 mL of a 0.1 M NaCl cell suspension containing 30 g (wet mass) of cell per liter. The cell suspensions were first adjusted to pH 3.0 using 1 M HCl, followed by a titration from pH 3.0 to 9.7 using 1 M NaOH that was used for calculating the total bindings sites on each sample using a four-site nonelectrostatic surface complexation model and FITEQL 2.0.36 All titrations were conducted in triplicate.

XANES and EXAFS Measurements. Te K-edge (31,814 eV) X-ray absorption spectroscopy measurements<sup>37</sup> were carried out at the MR-CAT/EnviroCAT bending magnet beamline (Sector 10, Advanced Photon Source).<sup>38</sup> X-ray absorption near edge spectra (XANES) and extended X-ray absorption fine structure (EXAFS) spectra were collected from the Te standards in transmission mode using gas-filled ionization chambers. The bacterial samples were measured in fluorescence using a four-element energy dispersive detector (Vortex). Biomass containing approximately 100 ppm of Te was harvested by centrifugation, and the hydrated cells were sealed between two layers of Kapton film in a 3 mm thick plexiglass well. Spectra were collected at room temperature inside a N<sub>2</sub>-purged sample cell using a 3 mm by 0.5 mm beam with a flux of approximately  $2 \times 10^9$  photons sec<sup>-1</sup>. Multiple quick scans were collected for the transmission samples, using 0.5 eV steps and 0.2 s dwell time per point. Slow scans were employed for the fluorescence spectra, using a 0.05 Å<sup>-1</sup> step size and a variable 1-4 s dwell time in the EXAFS region. Energy calibration was established by setting the inflection point in the spectrum from Te powder metal to 31 814 eV and then maintained continuously by collecting data from the reference simultaneously with the collection of data from the samples. Radiation-induced changes in the samples were monitored by taking quick XANES spectra and were not detected on the time scale of the EXAFS scans. No differences were observed between consecutive spectra and from several fresh areas on the samples so all scans from each sample were averaged to produce the final spectrum.

Analysis of the experimental spectra involved comparisons to Te standards, followed by numerical modeling of the data to extract the structural parameters describing the average atomic coordination around Te. Standards included disodium tellurate dihydrate powder (Strem Chemicals), disodium tellurite powder (Alfa Aeser), tellurium dioxide (TeO2) (Sigma-Aldrich), and Te(0) powder (Sigma-Aldrich). A Te-thiol standard was prepared using a thiol polymer (Purolite S924) with adsorbed tellurite (10 000 ppm and 1000 ppm). The powder Te standards were ground, sieved, and mounted on the adhesive side of Kapton tape, and folded 8 times at the beamline to produce an absorption edge of 0.5-1.0.37 Several scans were taken in transmission at three sample locationsthe lack of differences between the spectra indicated lack of significant pinhole effects or interaction of the minerals with the adhesive. The thiol polymer and biomass samples were mounted in 3 mm thick sample holders with Kapton windows. Normalization and background removal of the data was accomplished using the program AUTOBK.<sup>39</sup> The numerical analyses of the spectra are based on the crystal structures of disodium tellurite and TeO<sub>2</sub>. 40,41 The code FEFF8 42 was used to generate the single-scattering contributions in the EXAFS for the O, S, and Te coordination shells. Refinement of the numerical parameters against the experimental data was done in R-space using the program FEFFIT. 43

Protein Data Analysis. Publicly available B. subtilis proteomic data were analyzed to determine the cysteine content of cell wall, secreted, and surface-associated EPS proteins. The cell wall proteome, secretome, and cell surfaceassociated proteins were obtained from Antelmann and colleagues 44,45 and Otto et al.46 In these previous studies, B. subtilis was cultured in either Luria broth 44,45 or in a minimal medium with glucose as the carbon source.<sup>46</sup> In total, 739 unique proteins were analyzed. Protein sequences were downloaded in FASTA format from Uniprot, 47 and the abundance of cysteine residues was manually determined for each protein by counting the number of cysteines in the amino acid sequence. Subcellular localization of the proteins was predicted using CELLO and LocateP. 48,49 CELLO uses a twolevel Support Vector Machine system to assign localizations, while LocateP mimics protein targeting and secretion

processes and distinguishes protein export by general secretory and twin-arginine translocation pathways.

## ■ RESULTS AND DISCUSSION

Adsorption Isotherms. Reaction of aqueous tellurite with B. subtilis cells resulted in the loss of dissolved tellurium from solution (Figure 1). Adsorption experiments showed that the

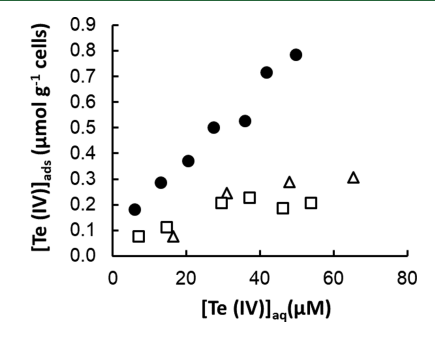


Figure 1. Tellurite adsorption isotherms. Adsorption of tellurite (Te[IV]) on to untreated Bacillus subtilis cells (●); cells treated with resin to desorb surface attached EPS ( $\Delta$ ); and cells treated with qBBr to block surface thiol sites ( $\square$ ). All experiments conducted at pH = 17.2.

concentration of adsorbed tellurite increased linearly with the aqueous tellurite concentration with a  $K_{\rm d}$  value of 19.5  $\pm$  5.4 L kg<sup>-1</sup>. To test if sulfhydryl sites are involved in tellurite adsorption, the membrane-impermeable thiol-specific probe qBBr was used to block the sulfhydryl sites on the bacterial surface. The adsorption isotherms showed significantly less tellurite adsorption by qBBr-treated cells compared to untreated cells. The partition coefficient of the qBBr-treated cells was  $K_d = 6.6 \pm 2.6 \text{ L kg}^{-1}$ . The decrease in the tellurite binding constant was attributed to tellurite binding to lowaffinity sites on the bacterial surface due to the loss of sulfhydryl complexation on the qBBr-treated cells. Finally, to test if the EPS were involved in tellurite adsorption, cells were treated with cation exchange resin to desorb the EPS attached to the cell surface. Removal of the EPS resulted in markedly less tellurite adsorption compared to untreated cells, with a  $K_d$ value of  $5.8 \pm 1.6 \text{ L kg}^{-1}$ . The extent of tellurite adsorption by resin-treated cells was similar to qBBr-treated cells suggesting that thiol functional groups in surface-associated EPS were involved in tellurite binding.

XANES and EXAFS. The XANES spectra of the reference compounds exhibited significant contrast between the different valence states and coordination environments of Te (Figure 2A). The oxidized Te(VI) species (Na<sub>2</sub>-tellurate) showed higher edge-energy positions, whereas the lower valent Te(IV) species (Na2-tellurite and TeO2) had lower edge energy positions with midpoints at 31 814.3 eV and 31 811.3 eV, respectively. Te(0) showed the same energy position as the two Te(IV) standards, but the spectrum had a significantly suppressed white line. Similar spectral dependence on Te valence has been previously observed. 7,8 To examine tellurite binding to sulfhydryl functional groups, we prepared a standard by reacting tellurite with a thiol-functionalized polymer. The Te-thiol standard showed the same edge position as the Ocoordinated Te(IV) standards, but the spectrum exhibited a suppressed white line intensity. The observed broadening and suppression of the white line for Te-S species relative to

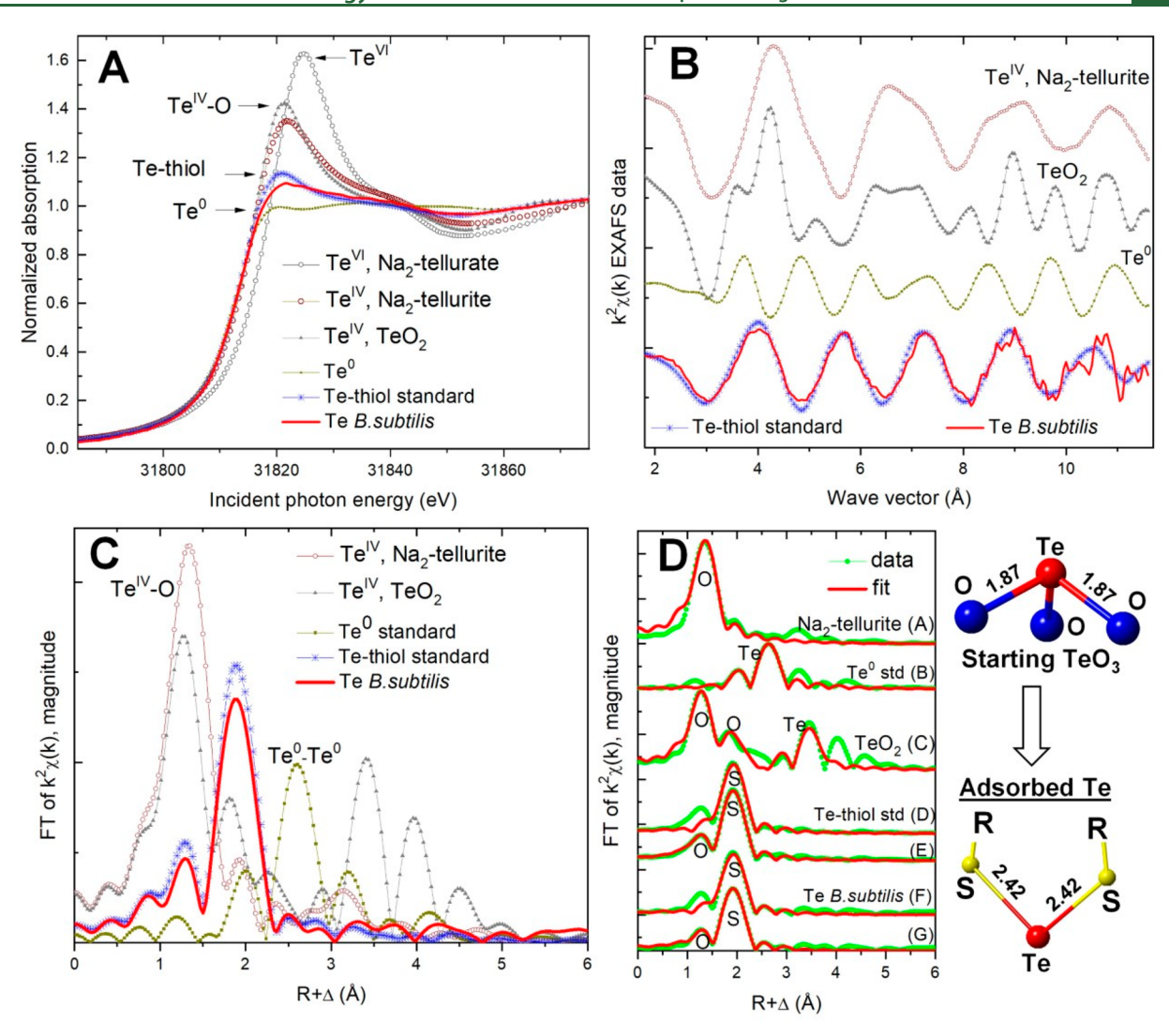


Figure 2. Te K-edge XAS of Te standards and Te adsorbed to *B. subtilis*. (A) XANES spectra. Arrows indicate the position and amplitude of the white lines for the different Te species; (B)  $k^2$ -weighed  $\chi(k)$  EXAFS spectra; (C) Fourier transform of the EXAFS data in the range  $\Delta k = 2.5-10.5$  Å<sup>-1</sup>; (D) Shell-by-shell fits of the EXAFS data. Letter designations (A–G) correspond to the EXAFS model listed in Table 1. The ball-and-stick models to the right illustrate the starting tellurite ion and the structure of the binding of the adsorbed Te atoms bound to S-based groups in the bindings.

species with O-coordination is similar to that observed with other elements (e.g., Fe, Ni, and Se). 50,51

Comparison of the *B. subtilis* sample to the XANES spectra of the standards indicated a change in Te coordination upon adsorption onto the bacterial surface (Figure 2A). The edge position of the *B. subtilis* spectrum was similar to the two Te(IV) standards, indicating that oxidation to Te(VI) did not occur. However, the XANES of Te adsorbed to *B. subtilis* was noticeably different from the Na<sub>2</sub>-tellurite standard. Most prominently, the white line of the *B. subtilis* spectrum was suppressed relative to the Na<sub>2</sub>-tellurite and TeO<sub>2</sub> standards. The XANES was also significantly different from that of Te(0) standard, indicating that reduction to elemental tellurium did not occur. The spectrum was most similar to that of Te adsorbed on the thiol polymer, suggesting that the Te was complexed to thiol ligands on the bacterial surface.

The EXAFS data showed that the Te of the tellurite adsorbed to *B. subtilis* was coordinated to sulfhydryl functional groups (Figure 2B,C). The spectrum of the *B. subtilis* sample was in excellent agreement with that of the Te-thiol standard

where sulfhydryl sites were the only available ligand. The B. subtilis spectrum was also substantially different in phase and amplitude from the Te(0) or the O-coordinated Te(IV) standards (Figure 2B). The Fourier transform (FT) of the  $\chi(k)$  data elucidated these differences, showing that the distance of the main peak was significantly different from that of the O-coordinated Te(IV) standards (Figure 2C). There was no amplitude in the B. subtilis spectrum where Te-Te coordination contribution was observed, indicating that tellurite reduction to Te(0) did not occur and that a precipitate with Te-Te coordination did not form. Linear combination fits of the data also indicated that metallic Te(0) was not present in the sample above the detection limits of EXAFS (Figure S1 of the Supporting Information, SI).

Shell-by-shell analysis was carried out to determine the local environment of Te in our samples and standards (fits A–G in Figure 2D and Table 1). The Na<sub>2</sub>-tellurite standard was successfully fit with a single shell of 3 O atoms at 1.87 Å (fit A), consistent with the structure of the isolated  ${\rm Te^{IV}O_3}$  anion in several  ${\rm Te(IV)}$  crystals.  $^{40,52,53}$  The refined  ${\rm S_0}^2$  factor of 0.93

Table 1. Fit Results for the EXAFS Data in Figure 2<sup>a</sup>

| shell                  | N                                     | R (Å)           | $\sigma^2 \ ({ m \AA}^2)$ | $\Delta E \; (\mathrm{eV})$ | DF | R-factor |
|------------------------|---------------------------------------|-----------------|---------------------------|-----------------------------|----|----------|
| (A) Na <sub>2</sub> To | eO <sub>3</sub> standard <sup>b</sup> |                 |                           |                             |    |          |
| O                      | $3.0 \pm 0.3$                         | $1.87 \pm 0.01$ | $0.0041 \pm 0.0012$       | $3.7 \pm 1.2$               | 3  | 0.006    |
| (B) Te me              | etal                                  |                 |                           |                             |    |          |
| Te                     | $2.3 \pm 0.2$                         | $2.83 \pm 0.01$ | $0.0064 \pm 0.0008$       | $10.3 \pm 0.6$              | 5  | 0.009    |
| (C) TeO <sub>2</sub>   | standard                              |                 |                           |                             |    |          |
| O                      | $1.8 \pm 0.6$                         | $1.83 \pm 0.02$ | $0.0028 \pm 0.0032$       | $-6.7 \pm 2.9$              | 6  | 0.036    |
| O                      | $7.5 \pm 2.0$                         | $2.58 \pm 0.05$ | $0.0200^c$                | $-6.7^{d}$                  |    |          |
| Te                     | $6.7 \pm 2.9$                         | $3.74 \pm 0.02$ | $0.0076 \pm 0.0035$       | $1.5 \pm 2.3$               |    |          |
| (D) Te-th              | iol standard                          |                 |                           |                             |    |          |
| S                      | $2.2 \pm 0.2$                         | $2.42 \pm 0.01$ | $0.0035 \pm 0.0009$       | $9.3 \pm 0.9$               | 5  | 0.008    |
| (E) Te-thi             | iol standard                          |                 |                           |                             |    |          |
| O                      | $0.6 \pm 0.2$                         | $1.79 \pm 0.03$ | $0.0026 \pm 0.0037$       | $-15.4 \pm 7.2$             | 4  | 0.004    |
| S                      | $2.1 \pm 0.2$                         | $2.42 \pm 0.01$ | $0.0035 \pm 0.0009$       | $9.6 \pm 0.9$               |    |          |
| (F) Te-bio             | omass data                            |                 |                           |                             |    |          |
| S                      | $2.0 \pm 0.2$                         | $2.42 \pm 0.01$ | $0.0038 \pm 0.0009$       | $9.7 \pm 0.8$               | 5  | 0.007    |
| (G) Te-bi              | omass data                            |                 |                           |                             |    |          |
| O                      | $0.3 \pm 0.1$                         | $1.82 \pm 0.03$ | $0.0000 \pm 0.0035$       | $-3.1 \pm 6.0$              | 4  | 0.004    |
| S                      | $2.0 \pm 0.2$                         | $2.42 \pm 0.01$ | $0.0041 \pm 0.0009$       | $9.3 \pm 1.0$               |    |          |

"N, R, and  $\sigma^2$  are coordination number, radial distance, and Debye-Waller factor, respectively, for each path used in the fit.  $\Delta E$  is the energy shift relative to the calculated Fermi level. DF = degrees of freedom in the fit, i.e., the difference between the number of independent data points and the number of fit parameters (data were fit between  $R + \Delta = 1.1 - 2.2$  Å for Na<sub>2</sub>-tellurite, 1.5 – 3.0 Å for metallic Te, 1.0 – 3.8 Å for TeO<sub>2</sub>, 1.5 – 3.0 Å for the Te(IV)-thiol and Te-biomass data). The R-factor is the fractional misfit of the data relative to its amplitude, and is a goodness-of-fit indicator. More details on these fit parameters can be found in FEFFIT's documentation<sup>43</sup>. <sup>b</sup>The amplitude suppression factor S<sub>0</sub><sup>2</sup> was determined to be 0.93 based on the fit of this standard where the O coordination is known to be 3.0; this  $S_0^2$  was then used in all other fits to refine the coordination numbers. Due to the overlapping contributions in this spectral region there was significant correlation between the coordination number and the Debye-Waller factor of this shell, so the latter was fixed to the value shown to stabilize the fit.  ${}^{d}$ The  $\Delta E$  variables for the two O shells were constrained to be the same

from this fit was used in all other fits to obtain the coordination numbers in the unknown spectra. The main peak in the Te(0) data was successfully fit with approximately 2 Te atoms at 2.83 Å (fit B), consistent with its crystal structure.<sup>54</sup> The TeO<sub>2</sub> standard was more complex due to the multiple possible allotropes in which the TeOx pyramids are distorted and connected to each other through one or two of the O atoms. 41,55,56 Our EXAFS data of TeO<sub>2</sub> reflects these distortions and connections, requiring two O shells and a Te shell model to fit the data (fit C). The inner O and the Te shells represent well the TeOx groups and the connections between them. The outer O shell attempts to capture the distorted and undefined coordination in between using a simplified single-shell model with a large Debye-Waller factor

Shell-by-shell analysis of the Te-thiol standard and B. subtilis sample indicated that the Te of the adsorbed tellurite had changed coordination and was bonded to ~2 sulfur atoms. The fits of the Te-thiol standard were based on the calculated structures of tellurite-sulfur glasses, in which S atoms replace O atoms in the chains of  $TeO_x$  entities in  $TeO_2$ . For the ab initio EXAFS calculation of a Te-S scattering path using FEFF8.2, the structure of TeO2 was modified by replacing the longer-distance O atoms at ~2.7 Å in the TeO<sub>x</sub> chains with S atoms. Figure 2D and Table 1 illustrate the fits of the EXAFS data from the Te-thiol standard (fit D) and B. subtilis sample (fit F) with S atoms coordinating Te at a distance of 2.42 Å. The remaining misfit around  $R + \Delta = 1.3$  Å could be compensated with an additional O shell (fits E and G). However, the refined Te-O distances were significantly shorter than those in the tellurite standard, suggesting that this peak was not due to unreacted tellurite. It is possible that this peak is due to an additional atom present in a Te-thiol

complex.<sup>59</sup> The interpretation of this spectral component does not change the fit of the major peak with a S shell, indicating that the predominant contribution to the main peak was from S atoms coordinating Te. Shorter distance (c.a. 2.4 Å), lower coordination (c.a. 2) S atomic environments have been observed for both Te(II)- and Te(IV)-thiol compounds, 55 whereas higher S-coordination (3–8 S) compounds exhibit Te–S distances of about 2.6–2.7 Å. <sup>59</sup> The refined coordination number of  $\sim$ 2 S atoms at 2.42  $\pm$  0.01 Å therefore suggests the formation of an inner-sphere RS-Te-SR complex on the bacterial surface (Figure 2D). The valence of the adsorbed Te could not be determined unequivocally from the Te-S distance, as both Te(II)- and Te(IV)-thiol compounds exhibit this distance.<sup>5</sup>

EPS Thiol Content. Because the adsorption data indicated that the thiol molecules in the EPS were involved in tellurite binding, we further investigated if proteins and sulfhydryl sites were present in the EPS of B. subtilis. Experiments were conducted to quantify the concentration of loosely attached proteins on the cell surface. The results indicated that proteinaceous EPS were present at all stages of growth (Figure 3A). The total concentration of surface attached proteins increased with time and corresponded to the growth of the culture. When normalized to cell numbers, the proteinaceous EPS density ranged from 2 to 16 fg of protein per cell.

Additional characterization of the EPS was performed to determine the thiol content. When reacted with mBBr, the proteinaceous EPS exhibited strong fluorescence indicating the presence of sulfhydryl sites (Figure 3B). Titration curves showed that the fluorescence emission increased steeply and linearly with the addition of mBBr until all the thiols in the sample were reacted with the fluorophore. After stoichiometric reaction with the sulfhydryl sites, the addition of excess mBBr

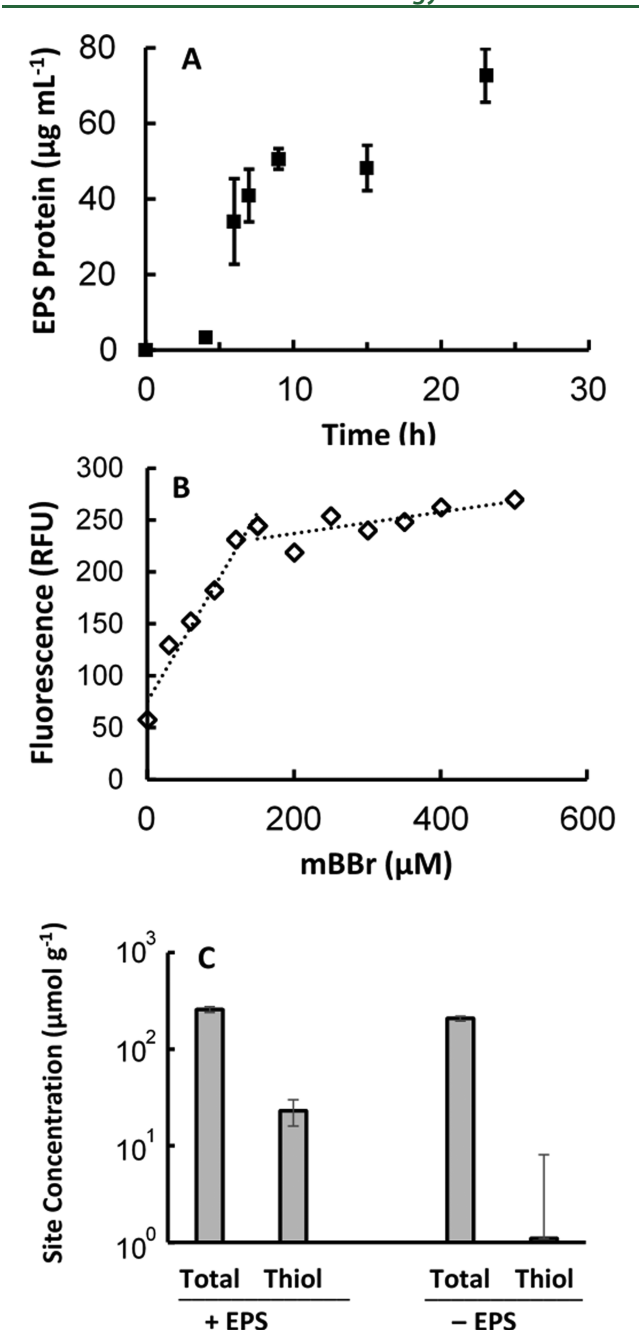


**Figure 3.** Protein and thiol content of *B. subtilis* EPS. (A) Protein concentration in EPS; (B) Thiol content of EPS collected from early stationary phase cultures. (C) Surface site concentrations of cells with intact EPS (+EPS) and cells with EPS removed (-EPS). Error bars represent the standard deviation of triplicate measurements.

resulted in a dampened fluorescence signal and a change in slope in the titration curve was observed. At the higher mBBr concentrations, the background fluorescence of the excess mBBr caused a shallow increase in fluorescence signal. The inflection point of the titration curve was used to determine the thiol concentration. Best fit lines of the two linear regions of the titration curve show an inflection point at  $143 \pm 24 \,\mu\text{M}$ . Normalized to wet weight, the thiol content of the EPS was  $21 \pm 4 \,\mu\text{mol}$  per gram of cells. Because mBBr does not react with disulfide bonds, these results demonstrate the presence of reduced thiols in the EPS that are in disequilibrium with the external oxidizing environment.

Finally, we performed titration experiments to confirm that the cell surface sulfhydryl sites were predominately associated with the EPS. Removal of the EPS from B. subtilis completely eliminated the cell surface thiol sites (Figure 3C). Acid-base titrations of cells with intact surface EPS showed a total surface site concentration of 257  $\pm$  17  $\mu$ mol g<sup>-1</sup>. Selective blocking of thiol sites using qBBr resulted in a 23  $\pm$  7  $\mu$ mol g<sup>-1</sup> decrease in total binding sites, representing the concentration of surface thiol functional groups. After the cell surface-associated EPS were detached, the sulfhydryl sites were no longer detectable as qBBr-blocking had no effect on surface binding site concentrations (p > 0.05 Student's t-test). Removal of surface-associated EPS decreased the total surface site concentration to 208  $\pm$  12  $\mu$ mol g<sup>-1</sup>, indicating that in addition to thiols sites, the EPS also contained other protonactive functional groups.

Molecular Mechanisms of Tellurite Adsorption. The data indicate that tellurite reacts with sulfhydryl functional groups in the EPS to form a RS-Te-SR structure (Figure 2D) similar to the organo-selenium components previously observed in selenite adsorption studies with B. subtilis. Although the EPS and cell surface are negatively charged at the neutral pH conditions of our experiments, our results indicate that the reaction between the sulfhydryl sites and the tellurite oxyanion is strong enough to overcome the electrostatic repulsive forces. We expect the electrostatic repulsive forces to decrease at lower pH values, thus increasing the extent of tellurite adsorption under acidic conditions. Upon binding to the sulfhydryl sites, the EXAFS spectra showed a change from shorter-distance Te-O coordination to a longer-distance Te-S coordination, with the adsorbed Te forming inner-sphere complexes with surface thiol groups (Figure 2D). The EXAFS data also indicate that the RS-Te-SR species are stable and do not condense in a precipitate with Te-Te coordination (Figure 2C).

The sulfhydryl-containing molecules in the EPS are currently unknown, but our results suggest that B. subtilis produces thiol-rich proteins that are involved in tellurite adsorption (Figure 3A,B). Because bacterial proteins that contain the amino acid cysteine harbor a sulfhydryl functional group, we analyzed publicly available B. subtilis proteomics data to elucidate the possible cysteine-containing molecules in the EPS. We compiled the data of Otto et al.<sup>46</sup> which identified over 600 proteins on the cell surface of B. subtilis using a biotinylation method. By analyzing the amino acid sequences, we found that many of these surface-associated proteins are highly enriched in cysteine (Table S1). The most cysteine-rich surface-associated protein is the dimodular nonribosomal peptide synthase DhbF which contains 16 cysteine residues. Also on the cell surface are the surfactin synthase subunits 1 and 2 which have 15 and 12 cysteines, respectively; the RNA polymerase RpoC with 11 cysteines; and FGAM synthase PurL with 10 cysteines. In total, we found that 466 of the surfaceassociated proteins contain cysteine (Table S1). Interestingly, these cysteine-containing proteins are predicted to have intracellular functions and their association with the EPS may be the result of lysis of dead cells in the bacterial culture. Cell lysis would also release cytoplasmic low molecular weight (LMW) thiols such as free cysteine and bacillithiol. LMW thiols are also known to be secreted by bacteria<sup>63</sup> and may make up a portion of the sulfhydryl sites within the EPS available for Te binding. Identifying the molecular hosts of sulfhydryl sites in the EPS merits further investigation.

Removal of the EPS dramatically decreased tellurite adsorption and the sulfhydryl surface site concentration (Figure 1 and 3C). Consistent with these observations, our analysis indicates that cell wall proteins of *B. subtilis* have no or very few cysteines (Table S2). Antelmann et al.<sup>45</sup> previously identified *B. subtilis* cell wall proteins that have specific wall-binding domains. Of these proteins, the cell wall-binding proteins YqgA and YwtD and the amidase enhancer LytB have the highest number of cysteine residues, each containing only two cysteines. All other cell wall proteins have one or no cysteines. Together with our experimental results, these low cysteine abundances suggest that the cell wall proteins are not the dominant molecules involved in tellurite binding.

Bioenvironmental Implications. The adsorption of Te(IV) and formation of stable RS-Te-SR components in the EPS are expected to affect bacterial Te(IV) uptake and microbial Te interactions. Previous studies of microbial Te(IV) reduction have largely focused on the chemical reactions that occur after Te enters the cells 16,17,64,65 and have neglected the mechanisms that control Te(IV) binding to the cell surface. Microorganisms can import tellurite into the cell and reduce Te(VI) to Te(0). 13,14 In environmental microbial systems, cell surface adsorption and uptake of tellurite are likely to co-occur to varying degrees depending on EPS production. Our results suggest that microorganisms that produce thiol-rich EPS would bind a significant portion of tellurite outside of the cell, thus limiting the translocation of Te into the cytoplasm and potentially mitigating the deleterious effects of tellurite uptake. <sup>13–15,66</sup> Alternatively, some *Bacillus* species use tellurite as an electron acceptor for anaerobic respiration 12 and tellurite binding to the EPS may impact tellurite availability to the electron transport chain. Te bound to EPS could also be transformed to Te(0) nanoparticles extracellularly, as subsequent reactions in the EPS can reduce RS-Te-SR to Te(0) similar to how thiolcarboxylic siderophores of Pseudomonas stutzeri convert tellurite to Te(0) via the formation of organotellurium intermediates. 30,67

Finally, our findings have important implications for understanding the environmental fate of Te adsorbed to bacterial surfaces. If high-affinity tellurite binding sites on bacteria are associated with loosely attached molecules on the cell surface, then the adsorbed organo-tellurium components can be released into aqueous solution as soluble organic matter when the EPS is destabilized. The attachment of EPS to cells is controlled, in part, by electrostatic interactions.<sup>68</sup> Thus, changes in environmental factors such as pH, salinity, and groundwater composition can trigger EPS detachment from the cell surface and render the organo-tellurium species mobile for transport. Of particular interest is the stability of cysteinerich proteins in the EPS which have high thiol site densities and likely have the greatest contribution to tellurite binding. The results of our study indicate that quantification of these sulfhydryl-containing molecules and the incorporation of protein-specific complexation reactions into surface complexation models will enable better predictions of how bacterial adsorption affects tellurite transport in landfills and other contaminated sites.

## ASSOCIATED CONTENT

# **5** Supporting Information

The Supporting Information is available free of charge at https://pubs.acs.org/doi/10.1021/acs.est.1c01001.

Linear combination analysis of the EXAFS data (PDF) Cysteine content of cell surface and cell wall proteins (XLSX)

Cysteine content of cell surface and cell wall proteins (XLSX)

#### AUTHOR INFORMATION

#### **Corresponding Author**

Nathan Yee — Department of Earth and Planetary Sciences, Rutgers University, Piscataway, New Jersey 08854, United States; Department of Environmental Sciences, Rutgers University, New Brunswick, New Jersey 08901, United States; orcid.org/0000-0002-1023-5271; Email: nyee@envsci.rutgers.edu

#### **Authors**

Jennifer L. Goff – Department of Earth and Planetary Sciences, Rutgers University, Piscataway, New Jersey 08854, United States

Yuwei Wang — Department of Environmental Sciences, Rutgers University, New Brunswick, New Jersey 08901, United States Maxim I. Boyanov — Bulgarian Academy of Sciences, Institute of Chemical Engineering, Sofia 1113, Bulgaria; Biosciences Division, Argonne National Laboratory, Argonne, Illinois 60439, United States; orcid.org/0000-0001-8758-5248

Qiang Yu — Department of Civil & Environmental Engineering & Earth Sciences, University of Notre Dame, Notre Dame, Indiana 46556, United States; orcid.org/0000-0001-5484-0927

Kenneth M. Kemner — Biosciences Division, Argonne National Laboratory, Argonne, Illinois 60439, United States Jeremy B. Fein — Department of Civil & Environmental Engineering & Earth Sciences, University of Notre Dame, Notre Dame, Indiana 46556, United States

Complete contact information is available at: https://pubs.acs.org/10.1021/acs.est.1c01001

#### Notes

The authors declare no competing financial interest.

## ACKNOWLEDGMENTS

This research was supported in part by grants EAR-1530089 and EAR-1904192 from the Geobiology and Low Temperature Geochemistry program within the U.S. National Science Foundation. Support was also provided by the Center for Environmental Science and Technology at University of Notre Dame. M.I.B. and K.M.K. were supported in part by the Subsurface Science Scientific Focus Area (SFA) at Argonne National Laboratory funded by the Subsurface Biogeochemical Research Program, Office of the Biological and Environmental Research, Office of Science, U.S. Department of Energy (DOE), under contract DE-AC02-06CH11357. MRCAT/EnviroCAT operations are supported by DOE and the MRCAT/EnviroCAT member institutions. Four anonymous reviewers provided insightful comments that greatly improved the manuscript.

## REFERENCES

(1) Zweibel, K. The impact of tellurium supply on cadmium telluride photovoltaics. *Science* **2010**, 328 (5979), 699–701.

(2) Zeng, C.; Ramos-Ruiz, A.; Field, J. A.; Sierra-Alvarez, R. Cadmium telluride (CdTe) and cadmium selenide (CdSe) leaching

- behavior and surface chemistry in response to pH and O2. J. Environ. Manage. 2015, 154, 78-85.
- (3) Ramos-Ruiz, A.; Wilkening, J. V.; Field, J. A.; Sierra-Alvarez, R. Leaching of cadmium and tellurium from cadmium telluride (CdTe) thin-film solar panels under simulated landfill conditions. J. Hazard. Mater. 2017, 336, 57-64.
- (4) Ramos-Ruiz, A.; Zeng, C.; Sierra-Alvarez, R.; Teixeira, L. H.; Field, J. A. Microbial toxicity of ionic species leached from the II-VI semiconductor materials, cadmium telluride (CdTe) and cadmium selenide (CdSe). Chemosphere 2016, 162, 131-138.
- (5) Ba, L. A.; Döring, M.; Jamier, V.; Jacob, C. Tellurium: an element with great biological potency and potential. Org. Biomol. Chem. 2010, 8 (19), 4203-4216.
- (6) Gerhardsson, L. Chapter 54-Tellurium. In Handbook on the Toxicology of Metals 4th ed.; Nordberg, G. F., Fowler, B. A., Nordberg, M., Eds.; Academic Press: San Diego, 2015; pp 1217-1228.
- (7) Qin, H.-B.; Takeichi, Y.; Nitani, H.; Terada, Y.; Takahashi, Y. Tellurium Distribution and Speciation in Contaminated Soils from Abandoned Mine Tailings: Comparison with Selenium. Environ. Sci. Technol. 2017, 51 (11), 6027-6035.
- (8) Harada, T.; Takahashi, Y. Origin of the difference in the distribution behavior of tellurium and selenium in a soil-water system, Geochim, Cosmochim, Acta 2008, 72 (5), 1281-1294.
- (9) Zannoni, D.; Borsetti, F.; Harrison, J. J.; Turner, R. J. The Bacterial Response to the Chalcogen Metalloids Se and Te. In Advances in Microbial Physiology; Poole, R. K., Ed.; Academic Press San Diego, 2007; Vol. 53, pp 1-312.
- (10) Kim, D. H.; Kanaly, R. A.; Hur, H. G. Biological accumulation of tellurium nanorod structures via reduction of tellurite by Shewanella oneidensis MR-1. Bioresour. Technol. 2012, 125, 127-31.
- (11) Zonaro, E.; Piacenza, E.; Presentato, A.; Monti, F.; Dell'Anna, R.; Lampis, S.; Vallini, G. Ochrobactrum sp. MPV1 from a dump of roasted pyrites can be exploited as bacterial catalyst for the biogenesis of selenium and tellurium nanoparticles. Microb. Cell Fact. 2017, 16
- (12) Baesman, S. M.; Bullen, T. D.; Dewald, J.; Zhang, D.; Curran, S.; Islam, F. S.; Beveridge, T. J.; Oremland, R. S. Formation of Tellurium Nanocrystals during Anaerobic Growth of Bacteria That Use Te Oxyanions as Respiratory Electron Acceptors. Appl. Environ. Microbiol. 2007, 73 (7), 2135-2143.
- (13) Elías, A.; Abarca, M. J.; Montes, R. A.; Chasteen, T. G.; Pérez-Donoso, J. M.; Vásquez, C. C. Tellurite enters Escherichia coli mainly through the PitA phosphate transporter. MicrobiologyOpen 2012, 1 (3), 259-267.
- (14) Elías, A.; Díaz-Vásquez, W.; Abarca-Lagunas, M. J.; Chasteen, T. G.; Arenas, F.; Vásquez, C. C. The ActP acetate transporter acts prior to the PitA phosphate carrier in tellurite uptake by Escherichia coli. Microbiol. Res. 2015, 177, 15-21.
- (15) Borghese, R.; Zannoni, D. Acetate Permease (ActP) Is Responsible for Tellurite (TeO<sub>3</sub><sup>2-</sup>) Uptake and Resistance in Cells of the Facultative Phototroph Rhodobacter capsulatus. Appl. Environ. Microbiol. 2010, 76 (3), 942.
- (16) Turner, R. J.; Aharonowitz, Y.; Weiner, J. H.; Taylor, D. E. Glutathione is a target in tellurite toxicity and is protected by tellurite resistance determinants in Escherichia coli. Can. I. Microbiol. 2001, 47
- (17) Turner, R. J.; Weiner, J. H.; Taylor, D. E. Tellurite-mediated thiol oxidation in Escherichia coli. Microbiology 1999, 145 (9), 2549-2557.
- (18) Garberg, P.; Engman, L.; Tolmachev, V.; Lundqvist, H.; Gerdes, R. G.; Cotgreave, I. A. Binding of tellurium to hepatocellular selenoproteins during incubation with inorganic tellurite: consequences for the activity of selenium-dependent glutathione peroxidase. Int. J. Biochem. Cell Biol. 1999, 31 (2), 291-301.
- (19) Laden, B. P.; Porter, T. D. Inhibition of human squalene monooxygenase by tellurium compounds: evidence of interaction with vicinal sulfhydryls. J. Lipid Res. 2001, 42 (2), 235-240.

- (20) Yu, Q.; Fein, J. B. Sulfhydryl Binding Sites within Bacterial Extracellular Polymeric Substances. Environ. Sci. Technol. 2016, 50 (11), 5498-5505.
- (21) Yu, Q.; Szymanowski, J.; Myneni, S. C. B.; Fein, J. B. Characterization of sulfhydryl sites within bacterial cell envelopes using selective site-blocking and potentiometric titrations. Chem. Geol. 2014, 373, 50-58.
- (22) Guiné, V.; Spadini, L.; Sarret, G.; Muris, M.; Delolme, C.; Gaudet, J. P.; Martins, J. M. F. Zinc Sorption to Three Gram-Negative Bacteria: Combined Titration, Modeling, and EXAFS Study. Environ. Sci. Technol. 2006, 40 (6), 1806-1813.
- (23) Mishra, B.; Boyanov, M.; Bunker, B. A.; Kelly, S. D.; Kemner, K. M.; Fein, J. B. High- and low-affinity binding sites for Cd on the bacterial cell walls of Bacillus subtilis and Shewanella oneidensis. Geochim. Cosmochim. Acta 2010, 74 (15), 4219-4233.
- (24) Mishra, B.; Boyanov, M. I.; Bunker, B. A.; Kelly, S. D.; Kemner, K. M.; Nerenberg, R.; Read-Daily, B. L.; Fein, J. B. An X-ray absorption spectroscopy study of Cd binding onto bacterial consortia. Geochim. Cosmochim. Acta 2009, 73 (15), 4311-4325.
- (25) Mishra, B.; Shoenfelt, E.; Yu, Q.; Yee, N.; Fein, J. B.; Myneni, S. C. B. Stoichiometry of mercury-thiol complexes on bacterial cell envelopes. Chem. Geol. 2017, 464, 137-146.
- (26) Yu, Q.; Boyanov, M. I.; Liu, J.; Kemner, K. M.; Fein, J. B. Adsorption of Selenite onto Bacillus subtilis: The Overlooked Role of Cell Envelope Sulfhydryl Sites in the Microbial Conversion of Se(IV). Environ. Sci. Technol. 2018, 52 (18), 10400-10407.
- (27) Kenward, P. A.; Fowle, D. A.; Yee, N. Microbial selenate sorption and reduction in nutrient limited systems. Environ. Sci. Technol. 2006, 40 (12), 3782-3786.
- (28) Fein, J. B.; Yu, Q.; Nam, J.; Yee, N. Bacterial cell envelope and extracellular sulfhydryl binding sites: Their roles in metal binding and bioavailability. Chem. Geol. 2019, 521, 28-38.
- (29) Albeck, A.; Weitman, H.; Sredni, B.; Albeck, M. Tellurium Compounds: Selective Inhibition of Cysteine Proteases and Model Reaction with Thiols. Inorg. Chem. 1998, 37 (8), 1704-1712.
- (30) Zawadzka, A. M.; Crawford, R. L.; Paszczynski, A. J. Pyridine-2,6-Bis(Thiocarboxylic Acid) Produced by Pseudomonas stutzeri KC Reduces and Precipitates Selenium and Tellurium Oxyanions. Appl. Environ. Microbiol. 2006, 72 (5), 3119.
- (31) Tan, I. S.; Ramamurthi, K. S. Spore formation in Bacillus subtilis. Environ. Microbiol. Rep. 2014, 6 (3), 212-225.
- (32) Joe-Wong, C.; Shoenfelt, E.; Hauser, E. J.; Crompton, N.; Myneni, S. C. B. Estimation of Reactive Thiol Concentrations in Dissolved Organic Matter and Bacterial Cell Membranes in Aquatic Systems. Environ. Sci. Technol. 2012, 46 (18), 9854-9861.
- (33) Perkins, W. T. Extreme selenium and tellurium contamination in soils — An eighty year-old industrial legacy surrounding a Ni refinery in the Swansea Valley. Sci. Total Environ. 2011, 412, 162-
- (34) Lowry, O. H.; Rosebrough, N. J.; Farr, A. L.; Randall, R. J. Protein measurement with the Folin phenol reagent. J. Biol. Chem. **1951**, 193 (1), 265–75.
- (35) Fahey, R. C.; Newton, G. L. Determination of low-molecularweight thiols using monobromobimane fluorescent labeling and highperformance liquid chromatography. Methods Enzymol. 1987, 143, 85-96.
- (36) Westall, J. C. FITEQL: A Computer Program for Determination of Chemical Equilibrium Constants from Experimental Data; Department of Chemistry, Oregon State University: Corvallis, OR, 1982.
- (37) Boyanov, M. I.; Kemner, K. M. Application of Synchrotron Xray Absorption Spectroscopy and Microscopy Techniques to the Study of Biogeochemical Processes. In Analytical Geomicrobiology: A Handbook of Instrumental Techniques; Alessi, D. S., Veeramani, H., Kenney, J. P. L., Eds.; Cambridge University Press:: Cambridge, MA, 2019; pp 238-261.
- (38) Kropf, A.; Katsoudas, J.; Chattopadhyay, S.; Shibata, T.; Lang, E.; Zyryanov, V.; Ravel, B.; McIvor, K.; Kemner, K.; Scheckel, K. The new MRCAT (Sector 10) bending magnet beamline at the advanced

- photon source. AIP Conference Proceedings; American Institute of Physics: College Park, MA, 2010, pp 299-302.
- (39) Newville, M.; Liviņš, P.; Yacoby, Y.; Rehr, J. J.; Stern, E. A. Near-edge x-ray-absorption fine structure of Pb: A comparison of theory and experiment. *Phys. Rev. B: Condens. Matter Mater. Phys.* **1993**, 47 (21), 14126–14131.
- (40) Masse, R.; Guitel, J.; Tordjman, I. Chemical Preparation and Crystalline-Structure of Sodium and Silver Tellurides Na<sub>2</sub>TeO<sub>3</sub>, AgTeO<sub>3</sub>. *Mater. Res. Bull.* **1980**, *15* (4), 431–436.
- (41) Thomas, P. A. The crystal structure and absolute optical chirality of paratellurite,  $\alpha$ -TeO<sub>2</sub>. *J. Phys. C: Solid State Phys.* **1988**, 21 (25), 4611–4627.
- (42) Ankudinov, A. L.; Ravel, B.; Rehr, J. J.; Conradson, S. D. Real-space multiple-scattering calculation and interpretation of x-ray-absorption near-edge structure. *Phys. Rev. B: Condens. Matter Mater. Phys.* 1998, 58 (12), 7565–7576.
- (43) Newville, M.; Ravel, B.; Haskel, D.; Rehr, J. J.; Stern, E. A.; Yacoby, Y. Analysis of multiple-scattering XAFS data using theoretical standards. *Phys. B* **1995**, 208–209, 154–156.
- (44) Antelmann, H.; Tjalsma, H.; Voigt, B.; Ohlmeier, S.; Bron, S.; van Dijl, J. M.; Hecker, M. A proteomic view on genome-based signal peptide predictions. *Genome Res.* **2001**, *11* (9), 1484–502.
- (45) Antelmann, H.; Yamamoto, H.; Sekiguchi, J.; Hecker, M. Stabilization of cell wall proteins in Bacillus subtilis: a proteomic approach. *Proteomics* **2002**, *2* (5), 591–602.
- (46) Otto, A.; Bernhardt, J.; Meyer, H.; Schaffer, M.; Herbst, F.-A.; Siebourg, J.; Mäder, U.; Lalk, M.; Hecker, M.; Becher, D. Systemswide temporal proteomic profiling in glucose-starved Bacillus subtilis. *Nat. Commun.* **2010**, *1* (1), 137.
- (47) Consortium, T. U. UniProt: a worldwide hub of protein knowledge. *Nucleic Acids Res.* **2019**, 47 (D1), D506–D515.
- (48) Yu, C.-S.; Chen, Y.-C.; Lu, C.-H.; Hwang, J.-K. Prediction of protein subcellular localization. *Proteins: Struct., Funct., Genet.* **2006**, 64 (3), 643–651.
- (49) Zhou, M.; Boekhorst, J.; Francke, C.; Siezen, R. J. LocateP: genome-scale subcellular-location predictor for bacterial proteins. *BMC Bioinf.* **2008**, *9*, 173.
- (50) Breynaert, E.; Bruggeman, C.; Maes, A. XANES-EXAFS analysis of se solid-phase reaction products formed upon contacting Se(IV) with FeS<sub>2</sub> and FeS. *Environ. Sci. Technol.* **2008**, 42 (10), 3595–601.
- (51) Jahrsengene, G.; Wells, H. C.; Sommerseth, C.; Ratvik, A. P.; Lossius, L. P.; Sizeland, K. H.; Kappen, P.; Svensson, A. M.; Haverkamp, R. G. An EXAFS and XANES Study of V, Ni, and Fe Speciation in Cokes for Anodes Used in Aluminum Production. *Metall. Mater. Trans. B* **2019**, *50* (6), 2969–2981.
- (52) Donnay, G.; Stewart, J.; Preston, H. The crystal structure of sonoraite, Fe<sup>3+</sup>Te<sup>4+</sup>O<sub>3</sub>(OH)·H<sub>2</sub>O. *TMPM, Tschermaks Mineral. Petrogr. Mitt.* **1970**, *14* (1), 27–44.
- (53) Miletich, R. Crystal chemistry of the microporous tellurite minerals zemannite and kinichilite,  $Mg_{0.5}$  [Me<sup>2+</sup> Fe<sup>3+</sup> (TeO<sub>3</sub>) 3]-4.5 H<sub>2</sub>O<sub>3</sub>(Me<sup>2+</sup> = Zn; Mn). *Eur. J. Mineral.* **1995**, 7, 509–524.
- (54) Adenis, C.; Langer, V.; Lindqvist, O. Reinvestigation of the structure of tellurium. *Acta Crystallogr., Sect. C: Cryst. Struct. Commun.* 1989, 45 (6), 941–942.
- (55) Beyer, V. H. Verfeinerung der Kristallstruktur von Tellurit, dem rhombischen TeO<sub>2</sub>. Acta Crystallogr. **196**7, 124 (3), 228–237.
- (56) Champarnaud-Mesjard, J.; Blanchandin, S.; Thomas, P.; Mirgorodsky, A.; Merle-Mejean, T.; Frit, B. Crystal structure, Raman spectrum and lattice dynamics of a new metastable form of tellurium dioxide:  $\gamma$ -TeO<sub>2</sub>. J. Phys. Chem. Solids **2000**, 61 (9), 1499–1507.
- (57) Mirgorodsky, A. P.; Soulis, M.; Thomas, P.; Merle-Méjean, T.; Smirnov, M. Ab initio study of the nonlinear optical susceptibility of TeO<sub>2</sub>-based glasses. *Phys. Rev. B: Condens. Matter Mater. Phys.* **2006**, 73 (13), 134206.
- (58) Jin, Z.; Biaggio, I.; Toulouse, J. Ab initio study of linear and nonlinear optical properties of mixed tellurite-chalcogenide glasses. *J. Phys.: Condens. Matter* **2010**, 22 (16), 165903.

- (59) Haiduc, I.; King, R. B.; Newton, M. G. Stereochemical Aspects of Tellurium Complexes with Sulfur Ligands: Molecular Compounds and Supramolecular Associations. *Chem. Rev.* **1994**, *94* (2), 301–326.
- (60) Fleischer, H.; Schollmeyer, D. Functionalized Tellurium(II) Thiolates: Tellurium Bis(2-hydroxyethanethiolate) Hydrate, the First H<sub>2</sub>O-Te<sup>II</sup> Complex. *Angew. Chem., Int. Ed.* **2000**, 39 (20), 3705–3706
- (61) Fleischer, H.; Schollmeyer, D. Conformation versus Coordination: Synthesis and Structural Investigations of Tellurium(II) Dithiolates Derived from  $\beta$ -Donor-Substituted Thiols. *Inorg. Chem.* **2002**, *41* (18), 4739–4747.
- (62) Fleischer, H.; Hennig, S.; Schollmeyer, D. Synthesis and Crystal Structure of Tellurium(II) bis(2-methoxycarbonylethanethiolate): A Novel Coordination Mode of Tellurium. *Z. Anorg. Allg. Chem.* **2003**, 629 (11), 1969–1974.
- (63) Owens, R. A.; Hartman, P. E. Export of glutathione by some widely used Salmonella typhimurium and Escherichia coli strains. *J. Bacteriol.* **1986**, *168* (1), 109–114.
- (64) Avazéri, C.; Turner, R. J.; Pommier, J.; Weiner, J. H.; Giordano, G.; Verméglio, A. Tellurite reductase activity of nitrate reductase is responsible for the basal resistance of Escherichia coli to tellurite. *Microbiology* **1997**, *143* (4), 1181–1189.
- (65) Moscoso, H.; Saavedra, C.; Loyola, C.; Pichuantes, S.; Vásquez, C. Biochemical characterization of tellurite-reducing activities of Bacillus stearothermophilus V. *Res. Microbiol.* **1998**, *149* (6), 389–397
- (66) Pérez, J. M.; Calderón, I. L.; Arenas, F. A.; Fuentes, D. E.; Pradenas, G. A.; Fuentes, E. L.; Sandoval, J. M.; Castro, M. E.; Elías, A. O.; Vásquez, C. C. Bacterial Toxicity of Potassium Tellurite: Unveiling an Ancient Enigma. *PLoS One* **2007**, 2 (2), e211.
- (67) Zawadzka, A. M.; Vandecasteele, F. P. J.; Crawford, R. L.; Paszczynski, A. J. Identification of siderophores of Pseudomonas stutzeri. *Can. J. Microbiol.* **2006**, 52 (12), 1164–1176.
- (68) Mayer, C.; Moritz, R.; Kirschner, C.; Borchard, W.; Maibaum, R.; Wingender, J.; Flemming, H. C. The role of intermolecular interactions: studies on model systems for bacterial biofilms. *Int. J. Biol. Macromol.* **1999**, 26 (1), 3–16.